Front. Chem. Sci. Eng. 2022, 16(1): 103–111
https://doi.org/10.1007/s11705-021-2064-8

RESEARCH ARTICLE

A highly selective fluorescent probe for real-time imaging of UDP-glucuronosyltransferase 1A8 in living cells and tissues

Mingyue Zhu[1,2*], Zhenhao Tian[3*], Lingling Jin[2], Xiaokui Huo[2], Chao Wang[2], Jingnan Cui[4], Yan Tian (✉)[2], Xiangge Tian (✉)[2], Lei Feng (✉)[1,2]

1 College of Pharmacy, School of Medicine, Key Laboratory of Elemene Class Anti-Cancer Chinese Medicines, Engineering Laboratory of Development and Application of Traditional Chinese Medicines, Hangzhou Normal University, Hangzhou 311121, China
2 Dalian Key Laboratory of Metabolic Target Characterization and Traditional Chinese Medicine Intervention, College of Pharmacy, College of Integrative Medicine, Dalian Medical University, Dalian 116044, China
3 School of Life Sciences, Northwestern Polytechnical University, Xi'an 710072, China
4 State Key Laboratory of Fine Chemicals, Dalian University of Technology, Dalian 116024, China

Abstract Uridine diphosphate (UDP)-glucuronosyltransferases (UGTs) are enzymes involved in the biotransformation of important endogenous compounds such as steroids, bile acids, and hormones as well as exogenous substances including drugs, environmental toxicants, and carcinogens. Here, a novel fluorescent probe BDMP was developed based on boron-dipyrromethene (BODIPY) with high sensitivity for the detection of UGT1A8. The glucuronidation of BDMP not only exhibited a red-emission wavelength ($\lambda_{ex}/\lambda_{em}$ = 500/580 nm), but also displayed an excellent UGT1A8-dependent fluorescence signal with a good linear relationship with UGT1A8 concentration. Based on this perfect biocompatibility and cell permeability, BDMP was successfully used to image endogenous UGT1A8 in human cancer cell lines (LoVo and HCT15) in real time. In addition, BDMP could also be used to visualize UGT1A8 in tumor tissues. These results suggested that BDMP is a promising molecular tool for the investigation of UGT1A8-mediated physiological function in humans.

Keywords UDP-glucuronosyltransferase 1A8, fluorescent probe, subtype selectivity, fluorescence imaging

1 Introduction

Uridine diphosphate (UDP)-glucuronosyltransferases (UGTs) are a family of phase II metabolic enzymes that play vital role in the metabolism of endogenous substrates (e.g., bilirubin, steroids, fatty acids thyroid hormones, and bile acids) and exogenous substrates (e.g., clinic drugs and environmental toxins) [1–5]. They catalyze the transfer of glucuronic acid from UDP-glucuronic acid (UDPGA) to various groups in drugs or xenobiotic such as hydroxyl, carboxyl, or amine groups [6–8]. Approximately 40%–70% of drugs can be metabolized by UGTs; moreover, the inhibition of UGTs also causes potential drug-drug interactions and disorders with endogenous substances [9]. UGTs are widely expressed in various organs in humans, animals, and plants. In humans, these species are located in the microsomal fraction of various tissues, including liver, kidney, skin, intestine, and brain [10]. To date, one hundred and seventeen members of the mammalian UGT gene superfamily has been reported; these were divided into four families: UGT1, UGT2, UGT3, and UGT8 [11,12]. Of these, UGT1 and UGT2 are the most studied families in the metabolism of endogenous and exogenous chemicals. In detail, the UGT1 family consists of nine isoforms, namely, UGT1A1, 1A3, 1A4, 1A5, 1A6, 1A7, 1A8, 1A9, and 1A10; the catalytic functions have all been well characterized. The UGT2B family is composed of six major isoforms, namely, UGT2B4, 2B7, 2B10, 2B11, 2B15, and 2B17.

The liver is an important metabolic organ with the greatest abundance of UGTs. The gastro-intestinal tract is also a significant extra-hepatic site for drug metabolism.

Received December 28, 2020; accepted April 6, 2021

E-mails: tiany2004@126.com (Tian Y), tianxiangge1990@163.com (Tian X), leifeng@dmu.edu.cn (Feng L)

*These authors contributed equally to this work.

Intestinal UGTs play a significant role in the changes of drug pharmacokinetics and drug-drug interactions [12,13]. Among various UGTs isoforms, UGT1A8 is an extra-hepatic drug metabolic UGTs isoform mainly expressed in the small intestine and colon [14,15]. UGT1A8 is a major enzyme in the elimination of endogenous estrogen [16]. A recent study indicated that UGT1A8 was closely related to the development of various cancers such as endometrial cancer and colorectal cancer [17]. Therefore, a sensitive and efficient detection tool for endogenous UGT1A8 is urgently needed for the relational use of drugs and for disease diagnosis.

Recently, small molecule fluorescent probes have been widely used for the rapid detection of enzyme activity, ions, pH, and reactive oxygen species. They have prominent advantages such as high sensitivity, non-invasiveness, and ultrahigh imaging resolution [18–30]. In humans, various metabolic enzymes play an important role in homeostasis, and their activity and dysregulation during disease have been compared to healthy subjects. Thus, enzyme-activated fluorescent probes are increasingly common for the real-time detection and imaging of key enzymes [31–35].

UGT1A8 is a significant UGT isoform that participates in the detoxification of environmental toxins and metabolites of drugs; surprisingly, few fluorescent probes for other subtypes of UGTs have been developed [36–38]. Unfortunately, there is no selective fluorescent probe for the detection of UGT1A8. Here, based on the optimal properties of boron-dipyrromethene (BODIPY), we designed a UGT1A8-activated fluorescent probe BDMP with good selectivity and stability and that exhibited ultrahigh imaging resolution in the imaging of UGT1A8 in various living cells and tissues (Scheme 1).

2 Experimental

2.1 Materials and reagents

The enzymes include UGT1A1, 1A3, 1A4, 1A6, 1A7, 1A8, 1A9, 1A10, 2B4, 2B7, 2B10, 2B15, and 2B17. These were all obtained from Corning Gentest (NY, USA). Bovine serum albumin, glutathione, serine, tryptophan, tyrosine, glutamate, glycine, arginine, cysteine, lysine, glutamine, myristic acid, and glucose were purchased from Shanghai Yuanye (Shanghai, China). Metal ions including Mg^{2+}, Ca^{2+}, Mn^{2+}, Ni^{2+}, Zn^{2+}, Sn^{4+}, K^{+}, Cu^{2+}, Fe^{3+}, Na^{+}, Ba^{2+}, Cr^{6+}, NO_3^{-}, CO_3^{2-}, and SO_4^{2-} were purchased from Shanghai Yuanye (Shanghai, China). Phenylbutazone, nilotinib, fluconazole, diclofenac, β-estradiol, deoxyschizandrin, hecogenin, magnolol, and propofol were purchased from J&K Chemicals (Beijing, China). LoVo cells and HCT15 cell lines were purchased from ATCC (Manassas, VA).

Nuclear magnetic resonance (NMR) spectra were analyzed on Bruker Avance II (400 MHz) spectrometer. All of the fluorescence tests were analyzed on Synergy H1 Microplate Reader (Bio-Tek). The reaction samples were analyzed by a Waters e2695 HPLC (high performance liquid chromatography) equipped with a photo-diode array detector. High-resolution mass data were measured on G6224A TOF MS. All of the other reagents and solvents used were of the highest grade commercially available.

2.2 Design and synthesis of BDMP for UGT1A8

Synthesis of compound **1**. Compound **1** was synthesized according to the literature [39]. The ^{1}H NMR data (400 MHz, $CDCl_3$) include: δ 7.64 (s, 1H), 7.20 (s, 1H), 6.93 (d, J = 2.9 Hz, 1H), 6.43 (s, 1H), 6.16 (s, 1H), 2.59 (s, 3H), and 2.28 (s, 3H) (Scheme S1, cf. Electronic Supplementary Material, ESM).

Synthesis of BDMP. Piperidine (170.3 mg, 2.0 mmol) and AcOH (120.1 mg, 2.0 mmol) were sequentially added to a dry toluene solution (20 mL) of compound **1** (44.0 mg, 0.2 mmol) and 2-bromo-3-hydroxy-4-methoxybenzaldehyde (55.2 mg, 0.24 mmol) under an argon atmosphere; the mixture was refluxed for 2 h. After removing the solvent, the residues were further purified by a silica gel column chromatograph using CH_2Cl_2/MeOH (100/1 v/v) as the mobile phase to afford BDMP as a dark red solid (69.7 mg, yield: 80.7%). ^{1}H NMR (400 MHz, DMSO-d_6, δ_{ppm}): 9.73 (s, 1H), 7.82 (t, J = 8.1 Hz, 2H), 7.73 (s, 1H),

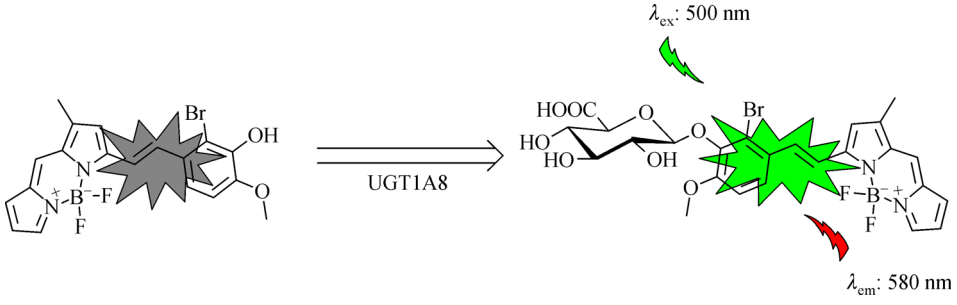

Scheme 1 The glucuronidation reaction of BDMP mediated by UGT1A8.

7.33 (d, J = 16.1 Hz, 1H), 7.27 (d, J = 8.6 Hz, 1H), 7.12 (dd, J = 8.8, 4.0 Hz, 3H), 6.53 (dd, J = 3.8, 2.0 Hz, 1H), 3.90 (s, 3H), 2.35 (s, 3H). ^{13}C NMR (100 MHz, DMSO-d_6, δ_{ppm}): 157.52, 149.63, 145.59, 144.17, 138.86, 138.53, 137.26, 132.97, 127.94, 126.70, 124.91, 118.14, 118.04, 117.47, 116.62, 112.31, 111.16, 56.25, and 11.06. HRMS (ESI negative) (high resolution mass spectrometry (electrospray ionization negative)): calcd. $[M - H]^-$ 431.0384, found 431.0392 (Figs. S1–S4, cf. ESM).

2.3 Incubation system for the *in vitro* assay

In the *in vitro* assay, all of the evaluations of UGT1A8 activity were performed in a standard incubation system including: 50 mmol·L^{-1} tris-HCl (pH 7.4), 50 mmol·L^{-1} $MgCl_2$, 40 mmol·L^{-1} UDPGA, fluorescent probe and recombinant UGT1A8 with a final incubation volume of 0.2 mL. After 3 min pre-incubation of fluorescent probe and enzyme, UDPGA was added as a cofactor to start the glucuronidation reaction, and incubated at 37 °C for another 30 min. Finally, the reaction was terminated upon addition of 100 μL ice-cold acetonitrile. The mixture was centrifuged at 4 °C at 20000 g for 20 min to remove the precipitate and retain the supernatant for further fluorescence experiments. The reaction samples were then analyzed by HPLC and mobile phases including A: 0.03% trifluoroacetic acid water; B: 100% MeOH. The gradient method was as follows: 0–10 min 80% A; 10–30 min 80%–10% A; 30–35 min 10% A; 35–40 min 10%–80% A; and 40–45 min 80% A. The flow rate was set to 0.8 mL·min^{-1}. Control incubations without enzyme were performed to ensure the metabolite formation was enzyme dependent.

2.4 Selectivity assays of BDMP

A selectivity assay was next performed to investigate whether BDMP possessed optimal selectivity toward UGT1A8. Briefly, BDMP (10 μmol·L^{-1}) was added into the assay system in the presence of 13 different isoforms of UGTs including UGT1A1, 1A3, 1A4, 1A6, 1A7, 1A8, 1A9, 1A10, 2B4, 2B7, 2B10, 2B15, and 2B17. The concentration of UGTs isoforms was set at 25 μg·mL^{-1} and incubated at 37 °C for 30 min, and then 100 μL ice-cold acetonitrile was added to stop the reaction for the fluorescence assay. To investigate the stability of BDMP, the influence of common metal ions (Mg^{2+}, Ca^{2+}, Mn^{2+}, Ni^{2+}, Zn^{2+}, Sn^{4+}, K^+, Cu^{2+}, Fe^{3+}, Na^+, Ba^{2+}, Cr^{6+}, NO_3^-, CO_3^{2-}, and SO_4^{2-}) were evaluated on BDMP along with glutathione, serine, tryptophan, tyrosine, glutamate, glycine, arginine, cysteine, lysine, glutamine, myristic acid, glucose; the concentration of metal ions and amino acids was 10 μmol·L^{-1}.

2.5 Chemical inhibition

To further confirm whether the fluorescence changes were selectively mediated by UGT1A8, different kinds of inhibitors of UGTs including phenylbutazone (500 μmol·L^{-1}), nilotinib (0.5 μmol·L^{-1}), gluconazole (2.5 mmol·L^{-1}), diclofenac (50 μmol·L^{-1}), β-estradiol (100 μmol·L^{-1}), deoxyschizandrin (20 μmol·L^{-1}), hecogenin (10 μmol·L^{-1}), magnolol (10 μmol·L^{-1}), and propofol (200 μmol·L^{-1}) were added to the reaction system [40–43]. The inhibition curve of different concentrations of nilotinib toward UGT1A8-mediated glucuronidation of BDMP was performed for a IC_{50} value. The inhibition activity was obtained by comparing the fluorescence intensity of the inhibitor group; the control group used blank solvent to replace the inhibitors.

2.6 Kinetic study

A kinetic study was performed to estimate the glucuronidation metabolism of BDMP. Here, BDMP (0–50 μmol·L^{-1}) was incubated with UGT1A8 for 30 min with a UGT1A8 concentration of 12.5 μg·mL^{-1}. Both incubation time and protein concentrations were selected within the linear interval to ensure that less than 20% of the substrate was metabolized and the formation of the glucuronidation metabolite was in the linear range [1,44,45]. Finally, the kinetic curve was fitting into the substrate inhibition formula (Eq. (1)) with the following formula:

$$v = \frac{V_{max}[S]}{K_m + [S] + [S]^2/K_i} \quad (1)$$

Here, V_{max} represents the maximum velocity; K_m is the substrate concentration at half-maximal rate, and K_i represents the dissociation constant of substrate binding to the inhibitory site. Kinetic curves were fitted using GraphPad Prism 6 and represent the mean ± SD.

2.7 Cell culture and fluorescence imaging

LoVo cells and HCT15 cells were cultured in RPMI-1640 medium supplemented with 10% fetal bovine serum (FBS) and maintained in 5% CO_2 at 37 °C. The cells were seeded on a 20 mm confocal dish and then cultured overnight. The media was then replaced with FBS-free media containing 2 μmol·L^{-1} BDMP and incubated for another 1 h. In the inhibition group, 20 μmol·L^{-1} nilotinib was pre-added into the cells and incubated with cells for 30 min in 5% CO_2 at 37 °C. The media was replaced with FBS-free media containing 2 μmol·L^{-1} BDMP and 20 μmol·L^{-1} nilotinib incubated with the remaining living cells for another 1 h under the same conditions. The culture media was then

discarded, and the cells were washed with phosphate buffer saline (PBS) three times and imaged on a confocal microscope (Leica TCS SP8).

2.8 Fluorescent imaging of cancer tissues slices

The tissue slices from colon tumors were prepared from frozen sections. The slices were incubated with 2 μmol·L^{-1} BDMP at 37 °C for 1 h, washed with PBS for 3 times, and then incubated with 4% paraformaldehyde at room temperature for 10 min. Finally, the cell nuclei were stained with 4,6-diamidino-2-phenylindole (DAPI)-containing Vecta shield solution (Vector Laboratories Inc.). The expression of UGT1A8 in tumors was imaged on a confocal microscope (Leica TCS SP8), and the conditions were consistent with the methods above.

3 Results and discussion

3.1 Spectrum response of BDMP toward UGT1A8

The spectroscopic properties change of BDMP after incubating with UGT1A8 were evaluated. As shown in Figs. 1(a) and 1(b), after metabolizing by UGT1A8, the absorption at 558 nm exhibited a significant enhancement, and a remarkable fluorescence signal was observed at 580 nm. In addition, in the HPLC analysis, we observed a new chromatographic peak in the incubation sample of BDMP in the presence of UGT1A8. The HRMS (ESI negative) was calculated for $C_{25}H_{23}BBrF_2N_2O_8^-$ that was found at *m/z* 607.0707 [M − H]$^-$, which corresponds to the glucuronidation product of BDMP (Fig. S5, cf. ESM). These results further confirmed the glucuronidation reaction for BDMP catalyzed by UGT1A8.

3.2 Fluorescence response of BDMP toward UGT1A8 at different concentrations

In order to accurately determine the activity of the target enzyme, it is necessary to investigate the relationship between fluorescence intensity and enzyme concentration. As shown in Fig. 2, the fluorescence intensity changes of BDMP mediated by UGT1A8 gradually increased and exhibited a good linear relationship with the increase of the concentration of UGT1A8 from 0 to 25 μg·mL^{-1} range. These results indicated that BDMP could serve as a novel tool for the real-time activity assaying of UGT1A8 in complex biosamples.

3.3 Selectivity study of BDMP toward UGT1A8

To investigate the selectivity of BDMP toward UGT1A8, the probe was incubated with 13 UGTs isoforms including UGT1A1, 1A3, 1A4, 1A6, 1A7, 1A8, 1A9, 1A10, 2B4, 2B7, 2B10, 2B15, and 2B17. As shown in Fig. 3, UGT1A1, 1A3, 1A7, 1A8, 1A9, and 1A10 could trigger the fluorescence enhancement of BDMP (Fig. 3(a)). Of these, UGT1A8 exhibited a relative prominent activity. In addition, as shown in Fig. 3(b), common endogenous

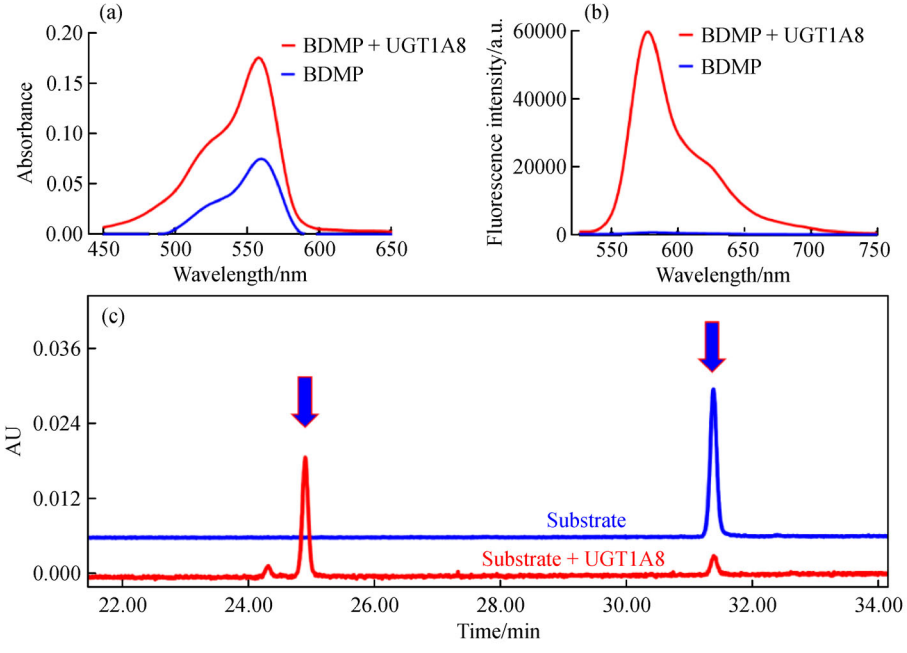

Fig. 1 (a) Absorption and (b) fluorescence emission spectra of BDMP (10 μmol·L^{-1}) before and after incubating with UGT1A8; (c) the HPLC analysis of BDMP and the incubation sample with UGT1A8.

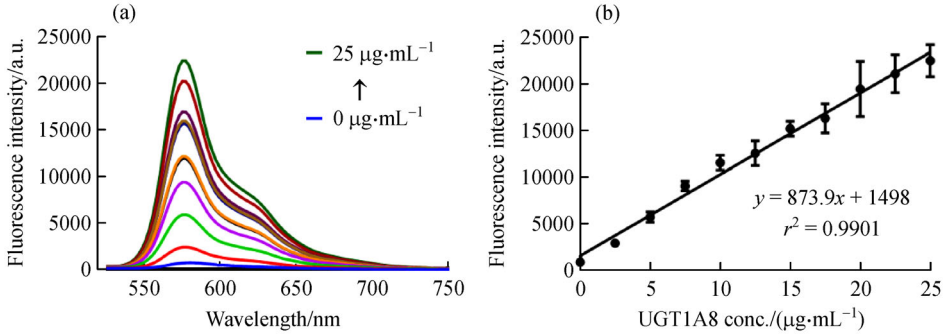

Fig. 2 (a) The fluorescence emission spectrum of BDMP (10 μmol·L^{-1}) after incubating with different concentrations of UGT1A8; (b) the linear regression of fluorescence intensity with UGT1A8 concentration.

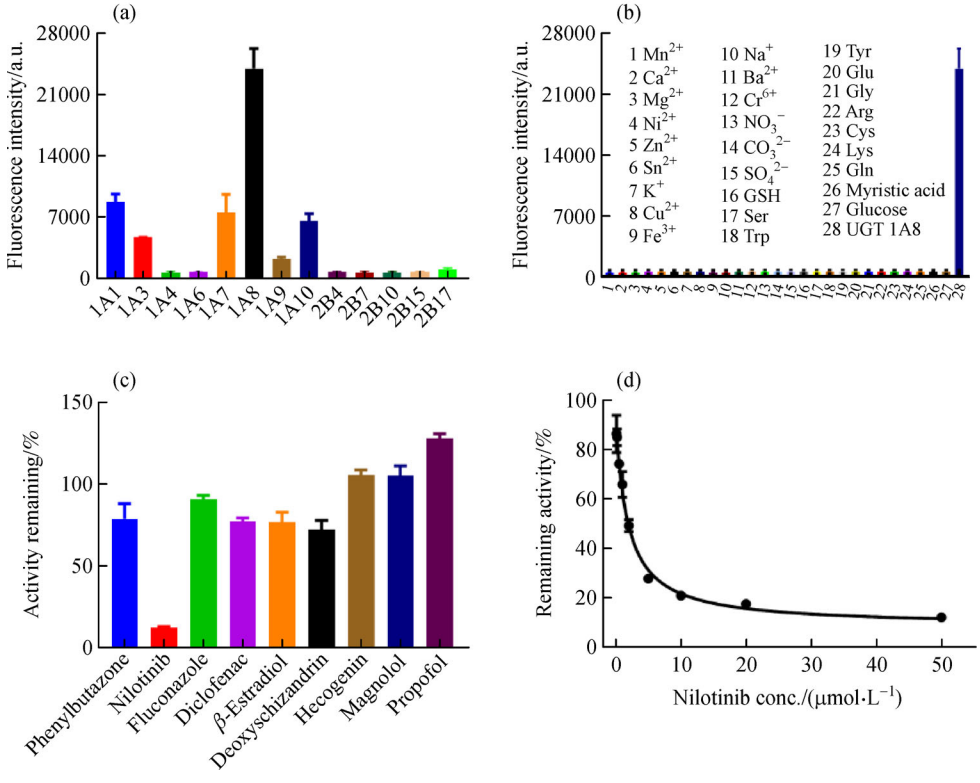

Fig. 3 (a) Fluorescence intensity of BDMP (10 μmol·L^{-1}) incubating with 13 isoforms of UGTs; (b) the stability of BDMP among metal ions and amino acids; (c) chemical inhibition of different inhibitors on UGT1A8 mediating the glucuronidation reaction; (d) the inhibition curve of Nilotinib toward the BDMP glucuronidation.

substances including metal ions and amino acids did not have any influence on the fluorescence signal of BDMP. Next, the effects of different chemical inhibitors on UGT1A8-mediated reactions were evaluated as shown in Fig. 3(c). Nilotinib had the strongest inhibitory effect on the reaction. The IC_{50} value of Nilotinib toward BDMP glucuronidation was 1.863 ± 0.037 μmol·L^{-1} (Fig. 3(d)). These results demonstrated that BDMP displayed a high selectivity toward UGT1A8 and could be used to determine the real biological activity of UGT1A8 in complex biological systems.

3.4 Kinetic study

To clarify the metabolism progress of BDMP, the kinetic behavior of BDMP glucuronidation in the presence of UGT1A8 was analyzed as shown in Fig. 4. The glucuronidation reaction had a substrate inhibition model

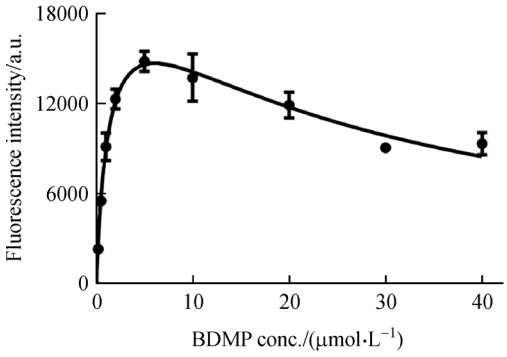

Fig. 4 The kinetic analysis of BDMP in the presence of UGT1A8.

kinetic for UGT1A8, and the dynamic parameters K_i and K_m were calculated to be 27.04 μmol·L^{-1} and 1.35 μmol·L^{-1}, respectively (Fig. 4). These results indicated that BDMP possessed excellent affinity toward UGT1A8, which provided assistance for the activity of UGT1A8 in complex biosamples.

3.5 Fluorescence imaging of BDMP in living cells and cancer tissues

UGT1A8 is an extrahepatic enzyme that is especially highly expressed in intestine, and plays a significant role in the detoxification of environmental carcinogens. Herein, BDMP was applied to image the activity of UGT1A8 in different colon cancers. First, a CCK8 cytotoxicity test showed that BDMP had no cytotoxicity to LoVo cells and HCT15 cells (Fig. S6, cf. ESM). Figure 5 showed that the fluorescence signal was detected in HCT15 cells after incubating with BDMP, which indicated that BDMP had excellent cell permeability; its biotransformation was mediated by endogenous UGT1A8. Furthermore, the UGTs inhibitor nilotinib could significantly suppress the fluorescence signal in living cells (Fig. 5(i)). The UGT1A8 could also be imaged in LoVo cells with BDMP (Fig. S7, cf. ESM). BDMP is a novel fluorescent probe for UGT1A8 and it has good imaging capabilities in the detection of intracellular UGT1A8. We next investigated cancer tissue imaging capabilities. Figure 6 showed that after incubating with BDMP for 1 h, the fluorescence signal was detected in the cytoplasm of cancer tissue slices. These results indicated that BDMP could be successfully used to detect endogenous UGT1A8 in tumor tissues and living cells.

4 Conclusions

In conclusion, a novel fluorescent probe BDMP for the detection of endogenous UGT1A8 was successfully developed using a BODIPY skeleton. BDMP could be metabolized by UGT1A8 to form a single glucuronidation metabolite, and possessed high sensitivity toward UGT1A8 on the basis of the isoform screening and chemical inhibition assay. Furthermore, BDMP exhibited excellent biocompatibility and could be further applied to real-time imaging of the endogenous UGT1A8 in various living cells and tissues. These findings demonstrate that BDMP is a promising tool for further investigation of the biological functions of endogenous UGT1A8 in many physiological and pathological processes.

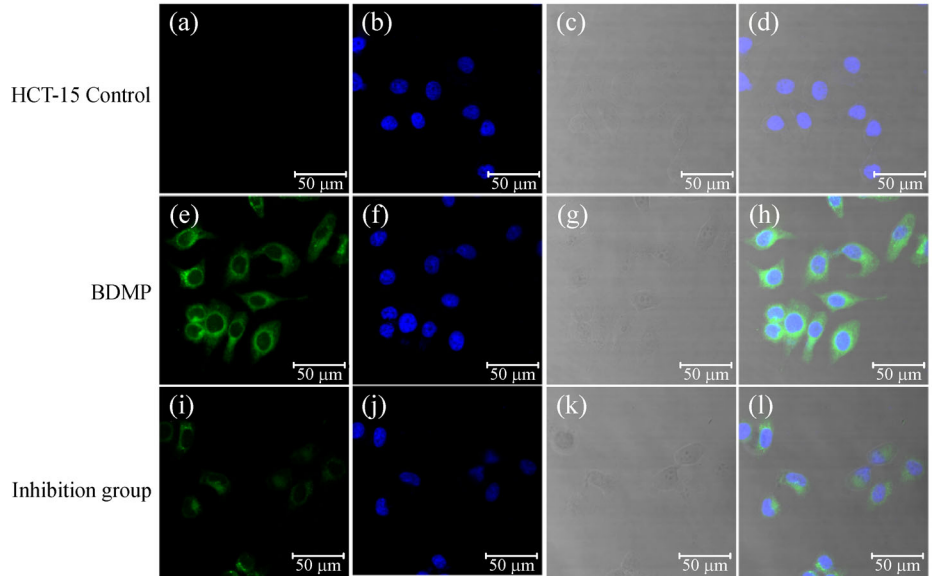

Fig. 5 (a, e, i) The fluorescence of HCT-15 cells; (b, f, j) staining of nuclei by Hoechst 33342; (c, g, k) bright field images of HCT15 cells; (d, h, l) merge of the confocal fluorescence images (The scale bar is 50 μm. BDMP: λ_{ex} 514 nm; λ_{em} 550–610 nm).

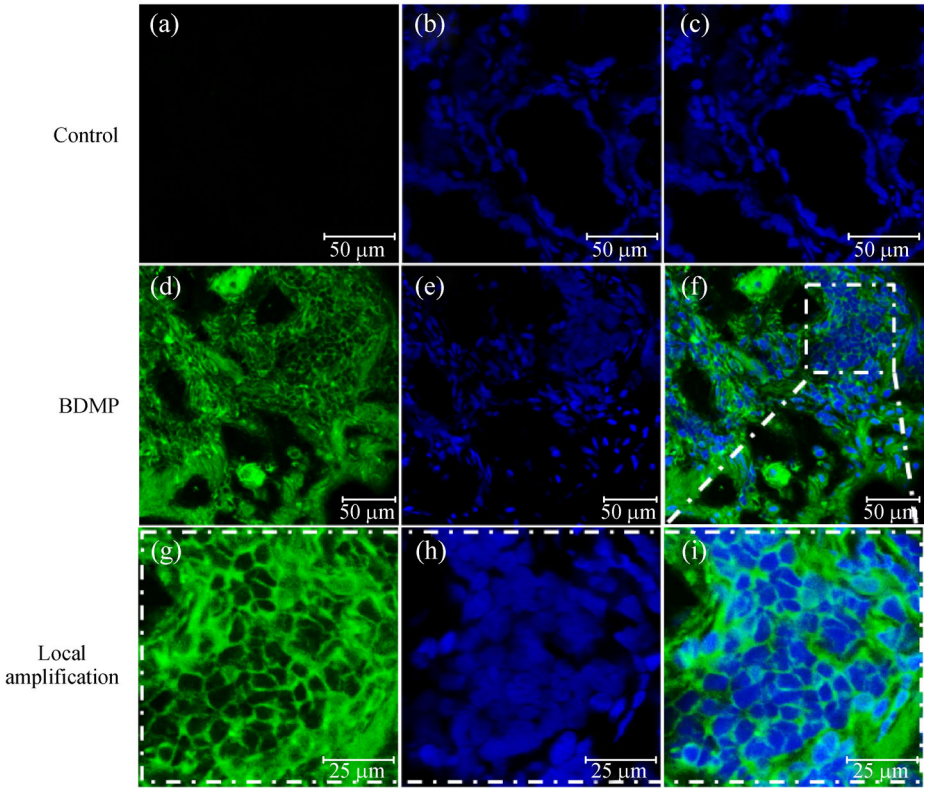

Fig. 6 (a, d, g) Fluorescence microscope imaging of UGT1A8 for the tissue slices of normal LoVo tumor tissues; (b, e, h) nuclear staining with DAPI; (c, f, i) merged confocal fluorescence images (The scale bars are 50 and 25 μm. λ_{ex} 514 nm; λ_{em} 550–610 nm).

Declaration of competing interest All the authors declare no competing financial interest.

Acknowledgments The authors thank the Natural Science Foundation of Liaoning Province 2020-MS-252 and the National Key R&D Program of China (Grant No. 2018YFC1603001).

Electronic Supplementary Material Supplementary material is available in the online version of this article at https://dx.doi.org/10.1007/s11705-021-2064-8 and is accessible for authorized users.

References

1. Tian X G, Liang S C, Wang C, Wu B J, Ge G B, Deng S, Liu K X, Yang L, Ma X C. Regioselective glucuronidation of andrographolide and its major derivatives: metabolite identification, isozyme contribution, and species differences. AAPS Journal, 2015, 17(1): 156–166
2. Kiang T K, Ensom M H, Chang T K. UDP-glucuronosyltransferases and clinical drug-drug interactions. Pharmacology & Therapeutics, 2005, 106(1): 97132
3. Oda S, Fukami T, Yokoi T, Nakajima M. A comprehensive review of UDP-glucuronosyltransferase and esterases for drug development. Drug Metabolism and Pharmacokinetics, 2015, 30(1): 30–51
4. Knights K M, Miners J O. Renal UDP-glucuronosyltransferases and the glucuronidation of xenobiotics and endogenous mediators. Drug Metabolism Reviews, 2010, 42(1): 63–73
5. Mu J, He L, Huang P, Chen X Y. Engineering of nanoscale coordination polymers with biomolecules for advanced applications. Coordination Chemistry Reviews, 2019, 399: 213039
6. Izukawa T, Nakajima M, Fujiwara R, Yamanaka H, Fukami T, Takamiya M, Aoki Y, Ikushiro S, Sakaki T, Yokoi T. Quantitative analysis of UDP-glucuronosyltransferase (UGT) 1A and UGT2B expression levels in human livers. Drug Metabolism and Disposition: the Biological Fate of Chemicals, 2009, 37(8): 1759–1768
7. Nakamura A, Nakajima M, Yamanaka H, Fujiwara R, Yokoi T. Expression of UGT1A and UGT2B mRNA in human normal tissues and various cell lines. Drug Metabolism and Disposition: the Biological Fate of Chemicals, 2008, 36(8): 1461–1464
8. Wu B J, Kulkarni K, Basu S, Zhang S X, Hu M. First-pass metabolism via UDP-glucuronosyltransferase: a barrier to oral bioavailability of phenolics. Journal of Pharmaceutical Sciences, 2011, 100(9): 3655–3681
9. Mackenzie P I, Bock K W, Burchell B, Guillemette C, Ikushiro S, Iyanagi T, Miners J O, Owens I S, Nebert D W. Nomenclature update for the mammalian UDP glycosyltransferase (UGT) gene superfamily. Pharmacogenetics and Genomics, 2005, 15(10): 677–685
10. Sanchez-Dominguez C N, Gallardo-Blanco H L, Salinas-Santander M A, Ortiz-Lopez R. Uridine 5′-diphospho-glucronosyltrasferase: its role in pharmacogenomics and human disease. Experimental and Therapeutic Medicine, 2018, 16(1): 3–11
11. Zhang R Y, Cui Y L, Wang Y, Tian X G, Zheng L, Cong H J, Wu B, Huo X K, Wang C, Zhang B J, Wang X, Yu Z. Catechol-*O*-

methyltransferase and UDP-glucuronosyltransferases in the metabolism of baicalein in different species. European Journal of Drug Metabolism and Pharmacokinetics, 2017, 42(6): 981–992

12. Xu M, Dong P P, Tian X G, Wang C, Huo X K, Zhang B J, Wu L J, Deng S, Ma X C. Drug interaction study of natural steroids from herbs specifically toward human UDP-glucuronosyltransferase (UGT) 1A4 and their quantitative structure activity relationship (QSAR) analysis for prediction. Pharmacological Research, 2016, 110: 139–150
13. de Boer Y S, Sherker A H. Herbal and dietary supplement—induced liver injury. Clinics in Liver Disease, 2017, 21(1): 135–149
14. Tukey R H, Strassburg C P. Human UDP-glucuronosyltransferases: metabolism, expression, and disease. Annual Review of Pharmacology and Toxicology, 2000, 40(1): 581–616
15. Tukey R H, Strassburg C P. Genetic multiplicity of the human UDP-glucuronosyltransferases and regulation in the gastrointestinal tract. Molecular Pharmacology, 2001, 59(3): 405–414
16. Lehmann L, Wagner J. Gene expression of 17β-estradiol-metabolizing isozymes: comparison of normal human mammary gland to normal human liver and to cultured human breast adenocarcinoma cells. Advances in Experimental Medicine and Biology, 2008, 617: 617–624
17. Zhao F, Wang X, Wang Y, Zhang J B, Lai R, Zhang B, Zhou X Y. The function of uterine UDP-glucuronosyltransferase 1A8 (UGT1A8) and UDP-glucuronosyltransferase 2B7 (UGT2B7) is involved in endometrial cancer based on estrogen metabolism regulation. Hormones (Athens, Greece), 2020, 19(3): 403–412
18. Tian X G, Yan F, Zheng J Y, Cui X L, Feng L, Li S, Jin L L, James T D, Ma X C. Endoplasmic reticulum targeting ratiometric fluorescent probe for carboxylesterase 2 detection in drug-induced acute liver injury. Analytical Chemistry, 2019, 91(24): 15840–15845
19. Tian X G, Liu T, Li L, Shao B, Yao D H, Feng L, Cui J N, James T D, Ma X C. Visual high-throughput screening for developing a fatty acid amide hydrolase natural inhibitor based on an enzyme-activated fluorescent probe. Analytical Chemistry, 2020, 92(14): 9493–9500
20. Wang Y, Yu F B, Luo X Z, Li M S, Zhao L L, Yu F B. Visualization of carboxylesterase 2 with a near-infrared two-photon fluorescent probe and potential evaluation of its anticancer drug effects in an orthotopic colon carcinoma mice model. Chemical Communications, 2020, 56(32): 4412–4415
21. Yang Y, Zhou T T, Jin M, Zhou K Y, Liu D D, Li X, Huo F J, Li W, Yin C X. Thiol-chromene "click" reaction triggered self-immolative for NIR visualization of thiol flux in physiology and pathology of living cells and mice. Journal of the American Chemical Society, 2020, 142(3): 1614–1620
22. Li H Y, Liu Y, Li X Y, Li X H, Ma H M. Design, synthesis and application of a dual-functional fluorescent probe for reactive oxygen species and viscosity. Spectrochimica Acta. Part A: Molecular and Biomolecular Spectroscopy, 2021, 246: 119059
23. Gurram B, Li M, Fan J L, Wang J Y, Peng X J. Near-infrared fluorescent probe for fast track of cyclooxygenase-2 in Golgi apparatus in cancer cells. Frontiers of Chemical Science and Engineering, 2020, 14(1): 41–52
24. Xu S Y, Sedgwick A C, Elfeky S A, Chen W B, Jones A S, Williams G T, Jenkins A T A, Bull S D, Fossey J S, James T D. A boronic acid-based fluorescent hydrogel for monosaccharide detection. Frontiers of Chemical Science and Engineering, 2020, 14(1): 112–116
25. Liu T, Tian M M, Wang J Y, Tian X G, Liu J H, Feng L, Ma X C, Cui J N. Rational design of a fluorescent probe for the detection of LAP and its application in drug-induced liver injury. Spectrochimica Acta. Part A: Molecular and Biomolecular Spectroscopy, 2021, 251: 119362
26. Liu H W, Chen L L, Xu C Y, Li Z, Zhang H Y, Zhang X B, Tan W H. Recent progresses in small-molecule enzymatic fluorescent probes for cancer imaging. Chemical Society Reviews, 2018, 47 (18): 7140–7180
27. Zhang J J, Chai X Z, He X P, Kim H J, Yoon J, Tian H. Fluorogenic probes for disease-relevant enzymes. Chemical Society Reviews, 2019, 48(2): 683–722
28. Wu X F, Shi W, Li X H, Ma H M. Recognition moieties of small molecular fluorescent probes for bioimaging of enzymes. Accounts of Chemical Research, 2019, 52(7): 1892–1904
29. Ning J, Liu T, Dong P P, Wang W, Ge G B, Wang B, Yu Z L, Shi L, Tian X G, Huo X K, et al. Molecular design strategy to construct the near-infrared fluorescent probe for selectively sensing human cytochrome P450 2J2. Journal of the American Chemical Society, 2019, 141(2): 1126–1134
30. Liu Z P, Sun Q. A near-infrared fluorescent probe for imaging of nitroxyl in living cells. Spectrochimica Acta. Part A: Molecular and Biomolecular Spectroscopy, 2020, 241: 118680
31. Ning J, Wang W, Ge G B, Chu P, Long F D, Yang Y L, Peng Y L, Feng L, Ma X C, James T D. Target enzyme-activated two-photon fluorescent probes: a case study of CYP3A4 using a two-dimensional design strategy. Angewandte Chemie International Edition, 2019, 58(29): 9959–9963
32. Feng L, Ning J, Tian X G, Wang C, Zhang L, Ma X C, James T D. Fluorescent probes for bioactive detection and imaging of phase II metabolic enzymes. Coordination Chemistry Reviews, 2019, 399: 213026
33. Ma H M. Spectroscopic Probes and Sensing Analysis. Beijing: Chemical Industry Press, 2020 (in Chinese)
34. Feng L, Ning J, Tian X G, Wang C, Yu Z L, Huo X K, Xie T, Zhang B J, James T D, Ma X C. Fluorescent probes for the detection and imaging of cytochrome P450. Coordination Chemistry Reviews, 2021, 437: 213740
35. Feng L, Tian Z H, Zhang M, He X, Tian X G, Yu Z L, Ma X C, Wang C. Real-time identification of gut microbiota with aminopeptidase N using an activable NIR fluorescent probe. Chinese Chemical Letters, 2021, https://doi.org/10.1016/j.cclet.2021.03.056
36. Terai T, Tomiyasu R, Ota T, Ueno T, Komatsu T, Hanaoka K, Urano Y, Nagano T. TokyoGreen derivatives as specific and practical fluorescent probes for UDP-glucuronosyltransferase (UGT) 1A1. Chemical Communications, 2013,49(30): 3101–3103
37. Lv X, Feng L, Ai C Z, Hou J, Wang P, Zou L W, Cheng J, Ge G B, Cui J N, Yang L. A practical and high-affinity fluorescent probe for uridine diphosphate glucuronosyltransferase 1A1: a good surrogate for bilirubin. Journal of Medicinal Chemistry, 2017, 60(23): 9664–9675
38. Kim B, Fukuda M, Lee J Y, Su D, Sanu S, Silvin A, Khoo A T T, Kwon T, Liu X, Chi W, Liu X, Choi S, Wan D S Y, Park S J, Kim J S, Ginhoux F, Je H S, Chang Y T. Visualizing microglia with a

fluorescence turn-on Ugt1a7c substrate. Angewandte Chemie International Edition, 2019, 58(24): 7972–7976

39. Lee J S, Kang N Y, Kim Y K, Samanta A, Feng S, Kim H K, Vendrell M, Park J H, Chang Y T. Synthesis of a BODIPY library and its application to the development of live cell glucagon imaging probe. Journal of the American Chemical Society, 2009, 131(29): 10077–10082
40. Huang Y P, Cao Y F, Fang Z Z, Zhang Y Y, Hu C M, Sun X Y, Yu Z W, Zhu X, Hong M, Yang L, Sun H Z. Glycyrrhetinic acid exhibits strong inhibitory effects towards UDP-glucuronosyltransferase (UGT) 1A3 and 2B7. Phytotherapy Research, 2013, 27(9): 1358–1361
41. Zhu L L, Ge G B, Liu Y, He G Y, Liang S C, Fang Z Z, Dong P P, Cao Y F, Yang L. Potent and selective inhibition of magnolol on catalytic activities of UGT1A7 and 1A9. Xenobiotica, 2012, 42(10): 1001–1008
42. He Y Q, Liu Y, Zhang B F, Liu H X, Lu Y L, Yang L, Xiong A Z, Xu L L, Wang C H, Yang L, Wang Z T. Identification of the UDP-glucuronosyltransferase isozyme involved in senecionine glucuronidation in human liver microsomes. Drug Metabolism and Disposition: the Biological Fate of Chemicals, 2010, 38(4): 626–634
43. Sahai J, Gallicano K, Pakuts A, Cameron D W. Effect of fluconazole on zidovudine pharmacokinetics in patients infected with human immunodeficiency virus. Journal of Infectious Diseases, 1994, 169 (5): 1103–1107
44. Yan F, Cui Y L, An Y, Ning J, Zhao X Y, Feng L, Huo X K, Wang C, Lv C Z, Ma X C, Tian X. A dual functional probe for assessing human CYP450 3A5 and 3A enzymes bioactivities. Future Medicinal Chemistry, 2019, 11(22): 2891–2903
45. Tian X G, Huo X K, Dong P P, Wu B J, Wang X B, Wang C, Liu K X, Ma X C. Sulfation of melatonin: enzymatic characterization, differences of organs, species and genders, and bioactivity variation. Biochemical Pharmacology, 2015, 94(4): 282–296